

Article

A Scalable Heat Pump Film with Zero Energy Consumption

Zhenghua Meng^{1,2} , Boyu Cao^{3,4}, Wei Guo^{1,2}, Yetao Zhong³, Bin Li³, Changhao Chen³, Hengren Hu³, Shigang Wu⁵ and Zhilin Xia^{3,*} 

¹ Hubei Key Laboratory of Advanced Technology for Automotive Components, Wuhan University of Technology, Wuhan 430070, China

² School of Automotive Engineering, Wuhan University of Technology, Wuhan 430070, China

³ State Key Laboratory of Silicate Materials for Architectures, Wuhan University of Technology, Wuhan 430070, China

⁴ School of Materials Science and Engineering, Wuhan University of Technology, Wuhan 430070, China

⁵ School of Materials Science and Engineering, Shandong University of Technology, Zibo 255049, China

* Correspondence: xiazhilin@whut.edu.cn

Abstract: Radiative cooling is an effective technology with zero energy consumption to alleviate climate warming and combat the urban heat island effect. At present, researchers often use foam boxes to isolate non-radiant heat exchange between the cooler and the environment through experiments, so as to achieve maximum cooling power. In practice, however, there are challenges in setting up foam boxes on a large scale, resulting in coolers that can be cooled below ambient only under low convection conditions. Based on polymer materials and nano-zinc oxide (nano-ZnO, refractive index > 2 , the peak equivalent spherical diameter 500 nm), the manufacturing process of heat pump film (HPF) was proposed. The HPF (4.1 mm thick) consists of polyethylene (PE) bubble film (heat transfer coefficient 0.04 W/m/K, 4 mm thick) and Ethylene-1-octene copolymer (POE) cured nano-ZnO (solar reflectance $\approx 94\%$ at 0.075 mm thick). Covering with HPF, the object achieves 7.15 °C decreasing in normal natural environment and 3.68 °C even under certain circumstances with high surface convective heat transfer (56.9 W/m²/K). HPF has advantages of cooling the covered object, certain strength (1.45 Mpa), scalable manufacturing with low cost, hydrophobic characteristics (the water contact angle, 150.6°), and meeting the basic requirements of various application scenarios.



check for updates

Citation: Meng, Z.; Cao, B.; Guo, W.; Zhong, Y.; Li, B.; Chen, C.; Hu, H.; Wu, S.; Xia, Z. A Scalable Heat Pump Film with Zero Energy Consumption. *Polymers* **2023**, *15*, 159. <https://doi.org/10.3390/polym15010159>

Academic Editors: Bożena Jarzabek, Ali Reza Zanjanijam and Agnieszka Wdowiak-Postulak

Received: 30 November 2022

Revised: 19 December 2022

Accepted: 24 December 2022

Published: 29 December 2022



Copyright: © 2022 by the authors. Licensee MDPI, Basel, Switzerland. This article is an open access article distributed under the terms and conditions of the Creative Commons Attribution (CC BY) license (<https://creativecommons.org/licenses/by/4.0/>).

Keywords: net zero energy consumption; radiation cooling; thermal insulation; polyethylene

1. Introduction

Carbon emissions are increasing year by year, which has become a worldwide urgent environmental issue. In 2020, for example, China's primary energy consumption reached 4.98 billion TCE, resulting in 9.9 billion tons of CO₂ emissions [1]. Researchers focus on finding solutions from environmentally friendly materials and natural materials that are commonly used in various fields such as energy storage [2–4] and photocatalysis [5–10] to alleviate environmental pressures. In recent years, there have been many remarkable results, such as: Zinatloo-Ajabshir et al. for the first time using banana extract, prepared under mild conditions with good hydrogen storage performance (after 20 cycles, the discharge capacity of 2611 mA h/g) pure Pr₂Ce₂O₇ nanostructures [2]. Cani et al. prepared a photocatalyst composed of C- and N-doped titanium dioxide (TiO₂) nanoparticles that can be reused continuously [11]. These achievements promote society towards a greener, more energy-efficient direction. However, with the improvement of people's living standards and climate change, the demand for refrigeration continues to be increasing. Approximately 1885 TWh electricity was used for space cooling in 2020, which accounted for 16% of the electricity consumption of the construction industry [12,13]. Additionally, refrigerators and air conditioners emitted CFCs that destroy the ozone layer, which causes the greenhouse effect and urban heat island effect [14]. Hence, developing climate friendly refrigeration technology draws the attention of researchers to alleviate environmental problems [15].

There is a window (8–13 μm) in the Earth's atmosphere that cannot capture infrared light, corresponding to the peak thermal radiation spectrum of terrestrial objects near ambient temperature (~ 300 K). With this transparent window, objects on Earth can radiate heat into the cold outer space (3 K), thereby cutting its own temperature [16]. Based on this principle, passive radiation cooling technology develops fast and has become a research hotspot recently because the whole cooling process is zero energy consumption. Many research results show that passive radiation materials achieve self-cooling and night cooling from surrounding objects [17–23]. However, the greatest demand for radiation cooling is in the daytime.

It is difficult to achieve cooling under the sunset only by relying on the thermal radiation performance of material itself, when the cooling materials absorb the solar radiation heat at the same time. It is an effective way to increase the selective radiation window and reduce the solar radiation absorption at the same time. Fan et al. [24] developed HfO_2 and SiO_2 photonic film structures, which had 97% solar reflectivity and achieved 4.9 $^\circ\text{C}$ cooling in direct sunlight. Recently, cooling coatings [25], woods [26], micro-structured photonic films [27], and fabrics [28] were developed through rational material selection as well as structural design. Besides, a few novel ideas have been generated with passive radiation cooling technology, such as self-cleaning passive radiation coolers [29], self-regulating passive radiation coolers [30,31], thermoelectric [32,33], water harvesting [34,35], solar panel cooling [36,37], cooling electronic devices [38], and water cooling devices of air conditioning [39].

Passive radiate cooling materials are divided into blackbody radiation materials [40–43] and selective radiation materials according to the radiation spectrum. As selective radiation materials, TPX (contains micrometer-sized SiO_2 spheres randomly distributed in the matrix material of polymethylpentene) [44], SiO_2 [45], SiCNO [46], CaMoO_4 [47], and some polymer materials [22,23] show good cooling potential when the objects placed in the circumstance without strong non-radiant heat exchange. Theoretically, if the solar absorption is suppressed and there is no non-radiative heat exchange, the cooling ability of 200 K can be achieved [48]. However, the actual non-radiative heat exchange is difficult to reduce to zero. In terms of non-radiative heat exchange, the cooling materials exchange heat with the environment through the top surface (on the environment side) and bottom surface (on the object side). Fan et al. [49] demonstrated that the sample's maximum temperature drop reached 42 K when the selective radiator was verified in a vacuum hood. In addition, to evaluate or use the cooling capacity of radiators, the foam box and PE cover film were used in experiments shown in Refs. [50–57]. The foam box covered with aluminum foil outside blocked the ambient temperature transferred into the sample, and PE film covered the above surface of the foam box blocked the interference of ambient convection. Once the test foam box and PE film cover were removed, the radiation cooler showed poor or zero cooling capacity. Lack of temperature preservation ability of radiation cooling materials, and the side-effect of non-radiative heat absorption, seriously limits the application of passive radiation cooling materials. By enhancing the thermal resistance of the bottom surface [51–61] and enlarging the radiation channel of the top surface, designing a multi-layer materials structure is a worthy solution to break the application limitations of radiation cooler. Wang et al. [62] prepared ultra-high foaming rate polyethylene aerogel with high solar reflectivity (92.2%, 6 mm thickness), high infrared transmittance (79.9%, 6 mm thickness), low thermal conductivity (28 mW/m/K) and was excellently insulated. The tests showed an excited result of a temperature drop of 13 $^\circ\text{C}$ at noon. However, the ultra-high foaming rate polyethylene aerogel has the disadvantages of poor strength and high manufacturing cost while it is hard to large-scale manufacture.

At present, there is no excellent solution to solve the problem that radiation cooling is not ideal in practical applications, and even cannot be cooled in high convective environments. Radiation cooling technology cannot get rid of the limitation of "foam box". This problem can be solved by isolating materials with high emissivity and high solar reflectivity. In fact, it is found that everything in nature carries out thermal radiation all the time. Using the object's own radiation capacity, by covering a layer of film, namely the heat pump film (HPF), the object's heat is like a pump to outer space with net zero energy consumption.

HPF is a two-layer material, which has advantages of cooling the covered objects, certain strength, prepared efficiently with minimal cost, hydrophobic characteristics, and meeting the basic requirements of diverse application scenarios.

2. Cooling Principle

A schematic diagram of the HPF structure and its working principle of heat exchange is shown in Figure 1A. The HPF has two layers with the whole infrared transparent: the top thin layer of material achieves high solar reflectivity; the bottom material is well insulated.

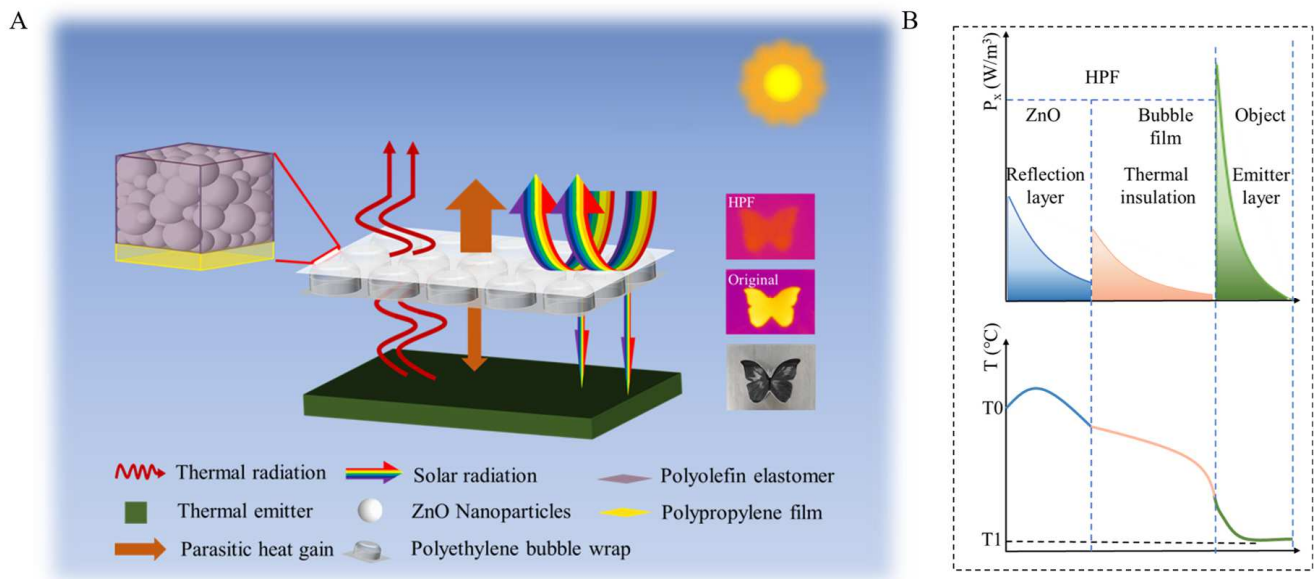


Figure 1. (A) Structural of HPF (ZnO film top layer and air bubble film bottom layer). (B) The cooling trend graph: The radiated power of each part of the material is distributed exponentially along the thickness direction.

Different with common radiate cooling emitters (thickness is <1 mm), whose cooling performance is usually analyzed by assuming that the temperatures on the upper and lower surfaces of the emitter are equal, the HPF (≈ 4 mm) has much higher thickness, up to the millimeter scale. There is a significant temperature difference between the upper and lower surfaces of the object, and the radiation distribution in the thickness direction needs to be considered. Light propagation is exponentially distributed along the thickness direction in an object (Figures 1B and S1). HPF is infrared transparent within the atmospheric window, but still has a weak radiative power. Hence, considering the radiation distribution of each part of the material, the overall heat dissipation of the radiator is defined as (Supplementary Information S1):

$$Q_{net} = Q_r - Q_a - Q_{nonrad} - Q_{sun} \quad (1)$$

where $Q_r = P_r ZnO + \varepsilon_2 P_r bubble\ film + \varepsilon_2 \varepsilon_3^n P_r object$ is the total radiated power emitted by the sample. ε_2 is the IR transmittance of the ZnO film and ε_3 is the IR transmittance of the bubble film (0.8). Q_a is the amount of incident atmospheric radiation absorbed by the sample. Q_{nonrad} is the non-radiative heat absorbed by the sample, which is generated by heat exchange through environmental convection and conduction, etc. ($Q_{nonrad} = h_c(T_{amb} - T_s)$, h_c is the non-radiative heat transfer coefficient between the environment and the radiant cooler, T_{amb} is ambient temperature and T_s is the temperature of the radiant cooler), Q_{sun} is the solar radiation absorbed by the sample.

The top layer is distributed Nano-powder with a high refractive index and low absorption. Selected materials with appropriate particle size can generate strong Mie scattering in the solar band without affecting the incidence in the atmospheric window band, resulting in high solar reflectivity (Q_{sun} is low) and infrared transmittance (8–13 μ m) simultaneously.

With the increase of solar absorption depth, the cooling effect becomes worse (Figure S2). Therefore, the use of a thin layer of material to reflect sunlight can greatly reduce the absorption of solar heat. The bottom layer is a bubble film with low thermal conductivity, which can block the heat conduction between the object and the environment. The bubble film is also infrared transparent. Hence, HPF has high solar reflection, infrared transmission in the 8–13 μm wavelengths, and low thermal conductivity. In addition, sufficient interface thermal resistance induced by the non-close contact between HPF and the object will also reduce the non-radiation heat transfer between the object and the environment (Q_{nonrad} is low). These conditions work together to ensure $Q_{\text{net}} > 0$.

3. Materials and Methods

3.1. Materials

Polypropylene (PP) film (25 μm thicknesses) was manufactured by Shenzhen Rongmaoda Electronic Materials Co., Ltd. PP is infrared (8–13 μm) transparent (Figure S3) and can be used as a reflective layer substrate.

ZrO₂, MgO, Al₂O₃, and ZnO nano-powders (the spherical equivalent peak diameter ≈ 500 nm) were manufactured by Hangzhou Hengna New Materials Co. The nano-powders are pure and free of other elements. Nano-powders with a high refractive index can undergo strong Mie scattering and achieve a high solar reflection effect. Here, ZnO Nano-powders, which have a refractive index of about 2 in solar wavelengths [63,64], also have the best IR transmission (Figure S4) and are selected to be the high solar reflection top layer. Based on Mie scattering theory, the size of ZnO particles is optimized. The normalized scattering cross section of ZnO nanoparticles was calculated (Figure S5). When the particle size is 100–1000 nm, the scattering cross section of visible and near infrared band is significantly improved, but the improvement of the atmospheric window band is not obvious. Reasonably, ZnO particles with the spherical equivalent diameter of 500 nm are selected (Figure S6). Besides, ZnO Nano-powders have an extinction coefficient being close to 0 in the 0.3–15 μm band, which means that the light absorption of the particles in these bands is very weak. Hence, the prepared ZnO film has nearly zero solar absorption, high solar band reflectivity, and a certain infrared (8–13 μm) transmission performance.

Polyethylene bubble film (PE bubble film, 2 mm thickness) was manufactured by Jiangmen Henghou Plastic Products Co. When PE films enclose air, the thermal conductivity of bubble film is only 0.04 W/m/K. The molecular structure of PE is composed of C-H and C-C bonds, which has no obvious absorption peak in the range of 8–13 μm brands. Hence, infrared transparent air and PE ensure the high transmittance of the bubble film in the atmospheric window (Figures 2A and S3).

Ethylene-1-octene copolymer (POE 7447) were manufactured by Dow Co. POE is often used as a toughening agent in modified PE or PP products. POE is infrared transparent in the atmospheric window band (Figure S3).

Petroleum ether (the boiling point: 60–90 °C) was manufactured by Macklin.

Polydimethylsiloxane (PDMS) Sylgard 184 was purchased from Dow Corning and is the ideal radiation cooler [65]. It comes as a two-part elastomer kit (the pre-polymer and curing agent).

3.2. Methods

Outdoor Test Platform: The test samples were placed on a PE foam box wrapped in aluminum foil. Aluminum foil reflects most of the sunlight and the foam box has low thermal conductivity to prevent external temperature intrusion into the radiation cooler from the bottom. The ambient temperature was measured by a Stevenson screen, and the temperature measurement data were exported by multi-channel temperature logger. Anemometer was used to measure the ambient humidity and temperature, and a Pyranometer was used to measure the solar radiation intensity.

Characteristic of Spectral Performance: The reflectance of ZnO films was measured with a UV-Vis NIR spectrophotometer (Lambda 750 S 200–25,000 nm) with an integrating sphere, and the IR transmittance of ZnO films, bubble film, and HPF were measured with

a Nicolet iS50 (Thermo Fisher, Waltham, MA, USA). The IR transmittance of building materials, PDMS, PE, and PP films were measured with a NEXUS Fourier transform infrared spectrometer (Thermo Fisher, Waltham, MA, USA). Part of the IR photographs was taken with an IR gun.

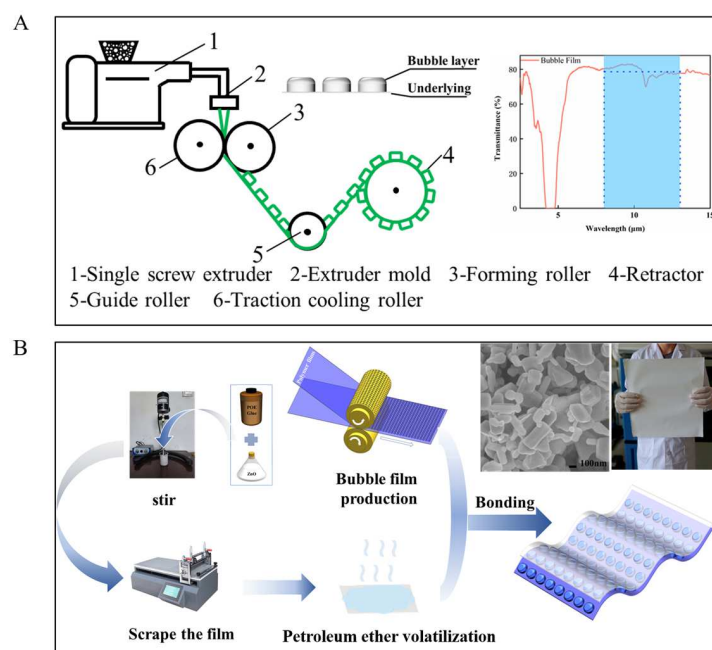


Figure 2. (A) Schematic diagram of the production process of PE bubble film, including measured transmittance of PE bubble film (2 mm thick) over MIR wavelength. (B) Schematic diagram of the production process of HPF, including the SEM photo of the upper surface of HPF.

Characteristic of Microscopic Morphology: Photographs of the particle distribution of ZnO film layers were taken by field emission scanning electron microscopy attached to a X-Max N80 energy spectrometer (JSM-7500F, JPN). The size of ZnO particles was tested by a laser particle sizer (Malvern ms3000, GBR).

Mechanical test: HPF tensile strength was tested by the Instron 5967 universal material testing machine.

3.3. HPF Preparation

PE bubble film is manufactured by the conventional large-scale extrusion blow molding process (Figure 2A). Under the condition of 50 °C water bath heating, 2.5 g POE7447 particles were dissolved in 50 mL petroleum ether to form POE glue. POE glue can be stable at room temperature and be beneficial to the subsequent process of ZnO powder. Then, 20 mL POE glue was combined with 10 g nano-ZnO particles and stirred for 2 h. The uniformly mixed solution is coated onto the PP substrate by a film scraping machine. ZnO film is formed after petroleum ether evaporation. ZnO film and PE bubble film are stuck together with POE glue to prepare the HPF (Figure 2A,B). The whole process of preparing HPF requires simple equipment, short preparation cycle, and even no high temperature environment. All materials used are easy to obtain and are cheap (Table S1).

4. Results and Discuss

4.1. Optical and Thermal Insulation Properties of HPF

To evaluate the effect of different ZnO film thicknesses and bubble film layers on the thermal performance, based on the optical test of HPF (Figure 3A,B), the calculation model of HPF was established (see Supplementary Information S1). The effects of thermal resistance and thermal radiation intensity on cooling performance were calculated by varying

the number of bubble film layers. The effects of solar reflectance and thermal radiation intensity on cooling performance were calculated by varying the ZnO film thickness. The calculation results are shown in Figure 3C,D.

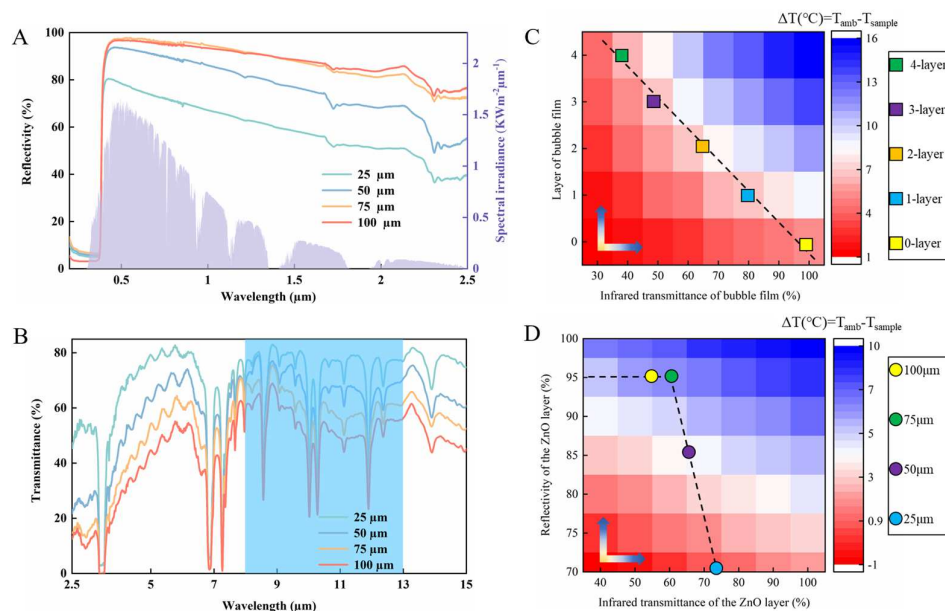


Figure 3. (A) Measured reflectance of different thicknesses of ZnO films over UV-VIS-NIR wavelengths, with the AM 1.5 solar spectrum. (B) Measured transmittance of different thicknesses of ZnO films over MIR wavelengths. (C) Model calculation: Setting the same object (PDMS, 200 μm) and ZnO (100 μm). Cooling results of object covered by 0–4 layers of bubble film. (D) Model calculation: Setting the same object (PDMS, 200 μm) and bubble film (2 layers). Cooling results of object covered by different thickness ZnO.

For the number of bubble film layers, it can be seen that one-layer or two-layer bubble film is the preferred choice for the cooling effect. The one-layer infrared transmittance of it in the atmospheric window is about 80% (Figure 2A). The thermal conductivity of bubble film is 0.04 W/m/K. The cooling capability of the sample with two-layer bubble film is already close to the optimal value that can be achieved.

For the thickness of ZnO, the infrared transmittance of the ZnO film decreases and the reflectance increases as the thickness increases in a range. Hence, the cooling performance of the HPF increases with the increase of ZnO thickness when solar radiates severely during the daytime. When it is greater than 75 μm, however, the thickness has little effect on the reflectance, while it has a side effect in IR transmittance. It will not be useful for the cooling performance of HPF. Outdoor experimental results validate the calculations (see Figures S7 and S8). In design and experiments, the preferred HPFs were prepared using two-layers of bubble film and 75 μm thickness ZnO film. Infrared transmission consequences of HPFs are shown in the Figure S9.

4.2. Characterization of HPF

Different from previous research works [28], columnar powder instead of sphere powder was selected to make ZnO film (Figure 2B), in order to low-cost scaled manufactured with low processing requirements. Some of the columnar particles reach micron size in the lengthwise direction, and the large size span of columnar ZnO is useful for achieving high reflectivity in a wider range of solar wavelengths. Although it affects the transmission in the atmospheric window band, fairly good cooling effect can be achieved. The SEM photos of the cross section (Figure 4) show the holes left by the volatilization of petroleum ether, which are conducive to the scattering of light. The POE is homogeneously mixed with ZnO particles to form a non-flaking film.

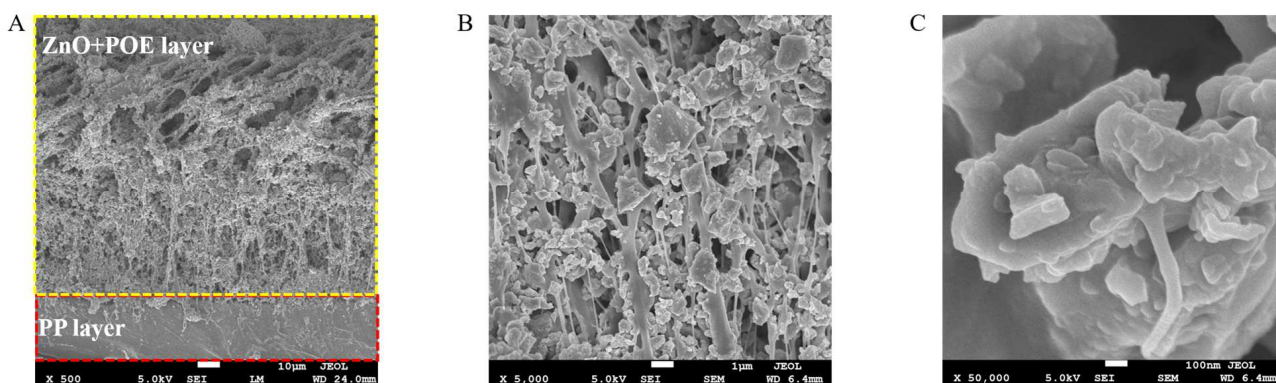


Figure 4. SEM photos of cross section of ZnO layer at different magnifications. (A) The scale is 1 mm. (B) The scale is 1 μm. (C) The scale is 100 μm.

4.3. Outdoor Cooling Test

4.3.1. Pump Heat without Auxiliary Heat Insulation

HPFs were prepared with 75 μm ZnO film and 4 mm bubble film, and a 24 h test was performed on covering on the PDMS coated Polyethylene terephthalate (PET) film (Figure 5A), where the infrared emission test of PDMS (200 μm) is shown in Figure S9. The experiments performed on a building roof in Wuhan, China (30°31'16.62" N, 114°20'46.32" E) on November 2021.

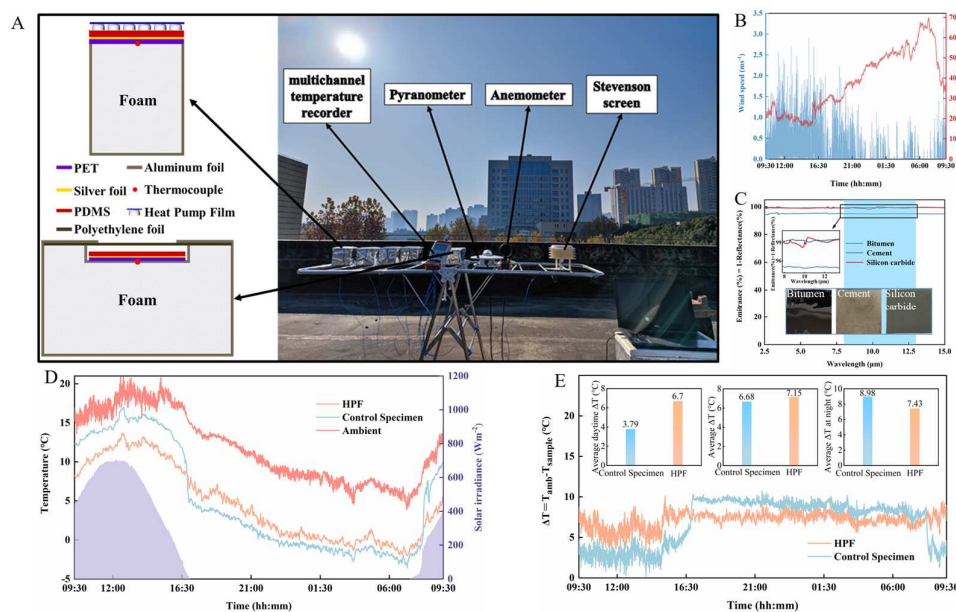


Figure 5. (A) Field test device, test location Wuhan, respectively, ambient temperature, sample temperature, wind speed, humidity, and solar radiation intensity, test device has temperature measurement device and control specimen device. (B) Wind speed and humidity testing during static roof testing. (C) Measured emissivity of building materials (bitumen, cement, and silicon carbide) over MIR wavelengths. (D) Sample temperature and ambient temperature testing under setup and control specimen setup, as well as real-time solar intensity testing. (E) Temperature variation of static roof test between device samples and control device specimen.

HPF was directly placed on the foam block and exposure to the environment, the test devices are shown in Figure 5A. For comparison, a control specimen with a foam box was tested at the same time. The commonly used foam box can hinder the non-radiative heat gain of the radiator and the environment, so the cooling capacity of the specimen in the foam box does not represent its effect in the natural environment. By abandoning the foam

box, the HPF experimental device is more in line with the actual application scenario, and the experimental results are more convincing.

The test results (Figure 5B,D,E) show that, the HPF-covered PDMS (HPF sample) could cool down an average 7.15 °C steadily within a day, and its cooling ability is still better than the control specimen (6.68 °C). Although the difference of two experimental results throughout the day is small, the HPF sample shows a more stable temperature dropping. Temperature variance calculations show (Figure S10) that the HPF sample has the smallest variance values ($S_{HPF} = 6.69, S_{transitional\ sample} = 8.3, S_{ambient} = 12.6$) compared with the ambient and the control specimen. The HPF with the low thermal conductivity (Figure S11), as the same as an air gap between the radiator and the environment created by the foam box, is also beneficial to reduce the non-radiative heat exchange between the radiator and the environment. Moreover, the HPF itself has high solar reflection performance, and advances in reducing influences by solar radiation. The foam box is easier to receive the solar radiation and warming during the daytime, resulting in a large difference in the average temperature drop of the internal radiator day and night. At the same time, a windless sub-environment was created with a transparent PE film wind shield to test the cooling of HPF. In this condition of low ambient convection, the HPF-covered PDMS object cooled down an average 11 °C during daytime (Figure S12). At the same time, the HPF outdoor experimental results are compared with the recent research (the optical property of the radiation cooler is similar), and the cooling effect is not much different (see Tables 1 and S2). The difference is that other studies use foam boxes to block the non-radiative heat exchange between the environment and the radiator, but the HPF test is not. HPF can be laid on a large scale on the outer surface of the building to achieve ideal cooling, while the large-scale installation of foam boxes is a challenge.

Table 1. Comparison between different testing devices [42,51].

Serial No.	Testing Device	Materials	Reflectance (%)	Emittance (%)	$\Delta T = T_{amb} - T_s$
(Wu L.) In a closed chamber		polymethyl methacrylate (PMMA)	95%	98%	6–8.9 °C
(Wang F.) with wind shield		BaSO ₄ and SiO ₂	95%	96%	6.2 °C
HPF without wind shield	See Figure 4A	PDMS and HPF	≈94%	97%	7.15 °C

4.3.2. Pump Heat Covered on Different Materials

Cooling tests on traditional building materials (such as bitumen, cement, and silicon carbide) were also conducted (Figures 5C and S13). HPF can reflect sunlight greatly, so even pure black bitumen can achieve cooling below the ambient temperature when covered by HPF. Despite the different thicknesses of the three materials (Silicon carbide ≈ 200 μm, Bitumen ≈ 500 μm, Cement ≈ 2 mm), the cooling effect does not differ much (all can achieve >5 °C cooling) because their emissivity in the atmospheric window band does not differ much ($\epsilon_{Bitumen} \approx 0.95, \epsilon_{Cement} \approx 0.99, \epsilon_{Silicon\ carbide} \approx 0.99$).

In fact, almost all natural objects have a high radiation capacity when they are thick enough. However, the objects cannot cool down during the day due to solar absorption. When covered by HPF, almost all materials tend to cool down to a certain extent, depending

on their own properties (see Figure S14). It is believed that HPF can satisfy most ordinary objects for providing heat pump cooling.

4.3.3. Pump Heat under Strong Convection Environment

The HPF cooling performance under a high convection environment was tested. A PDMS object covered by HPF was fixed steadily on the roof of a driving car with an average speed of 70 km/h. The surface heat transfer coefficient (h_s) of the object is about $56.9 \text{ W/m}^2/\text{k}$. The temperature change test results show that, the object cooled down an average $3.5 \text{ }^\circ\text{C}$ in a 40 minute journey (Figure S15).

In Formula 1, $Q_{nonrad} = h_c(T_{amb} - T_s)$. For radiant coolers, h_c satisfies the empirical formula [66]: 1. For a set-up without a wind shield, $h_{c1} = 8.3 + 2.5v$; 2. For a set-up with a wind shield, $h_{c2} = 2.5 + 2v$; 3. In a closed chamber, $h_{c3} = 2.5 \text{ W/m}^2\text{K}$. v is the wind speed, m/s. For the HPF covered radiant coolers, $h_c = \frac{1}{R+(1/h_{c1})}$, R is the thermal resistance of the HPF, $R= 0.1 \text{ m}^2\text{K/W}$. Based on the work of other researchers, Table 2 was plotted. It can be seen that, when out of the foam box, the cooling effect of the radiation cooler is much worse. The data in bold font format are calculated based on the original paper data (assuming that the non-radiative heat transfer power of different environments is the same). The radiation cooler without wind shield cools $<3 \text{ }^\circ\text{C}$ when v is just set to 1 m/s. However, the cooler under HPF can still be cooled $3.5 \text{ }^\circ\text{C}$ even with a wind speed of 19 m/s (Speed 70 Km/h) due to its low thermal conductivity. There is little research to achieve cooling in a highly convective environment without a foam box.

Table 2. Cooling results in different environments.

Serial No.	In a Closed Chamber	With Wind Shield	Without Wind Shield
(Wu L.)	6–8.9 $^\circ\text{C}$	3.3–4.9 $^\circ\text{C}$	1.4–2.1 $^\circ\text{C}$
(Wang F.)	×	6.2 $^\circ\text{C}$	2.6 $^\circ\text{C}$
HPF	×	×	7.15 $^\circ\text{C}$

To explore the effect of h_s on cooling, the cooling effect of HPF was calculated (Figures 6A,B and S16) based on Supplementary Information S1. PDMS film was used as the object to analyze the cooling effect of the HPF. h_s is set between ($10\text{--}80 \text{ W/m}^2/\text{k}$), and the number of bubble film layers number is set to (0–4).

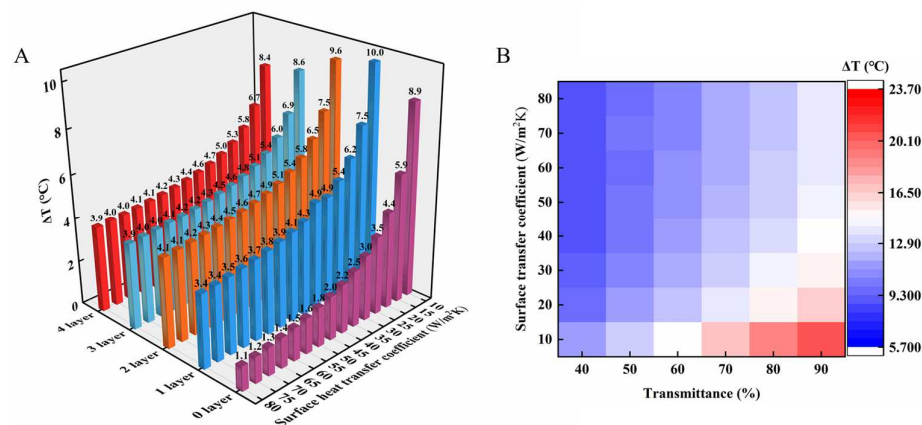


Figure 6. (A) Model calculation: cooling histogram of samples with different h_s and different layers of bubble film insulation. (B) Model calculation: cooling forecast hotspot diagram with different h_s and different transmittance (8–13 μm) of HPF.

The results show that, when the h_s is lower than $40 \text{ W/m}^2/\text{k}$, the cooling ability of the HPF gradually decreases with the increase of h_s . It will basically remain stable when h_s is

larger than $40 \text{ W/m}^2/\text{k}$. In this situation ($h_s > 40 \text{ W/m}^2/\text{k}$), the PDMS object covered by HPF cools down more than $3.4 \text{ }^\circ\text{C}$. In contrast, the PDMS object covered by ZnO film only cools down about $1 \text{ }^\circ\text{C}$. Besides, different with the low h_s situation test results, the layers number of bubble film of HPF has little influence of cool ability. It is considered that this is because the transmittance, heat insulation, and radiation performance are changed accordingly.

It shows that there is still room for performance improvement for HPF (Figure 6B). The infrared transmittance at $8\text{--}13 \text{ }\mu\text{m}$ of the HPF cooler is being optimized and improved. According to deduction, HPF could cool down the covering objects to about $24 \text{ }^\circ\text{C}$, if some methods are adopted to increase the transmittance of HPF to 90%, such as applying spherical ZnO particles and fabricating with a complex fine mixing process.

4.4. Additional Performance

As previous research [62] showed, the infrared transparent polyethylene aerogel (PEA) has better characteristics (6 mm thickness, solar reflectance 92.2%, infrared transmittance 79.9%, thermal conductivity 28 mW/m/K) and $13 \text{ }^\circ\text{C}$ cooling ability at noon. However, it has insufficient mechanical properties after freeze-drying preparation, which may be restricted to apply. HPF should maintain certain strength in practical application. The tensile test results showed that the tensile strength of HPF reached 1.45 Mpa, which was significantly higher than that of PEA (Figures 7A and S17). HPF shows good flexibility and bendability: The nanoparticles adhere closely without peeling even if the ZnO film is folded into a cranes shape.

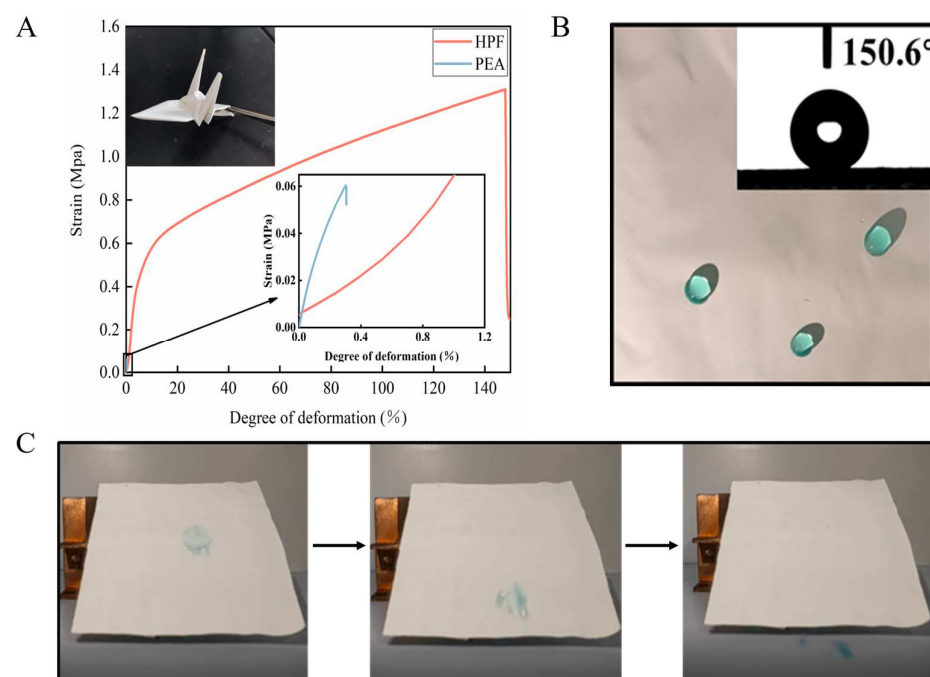


Figure 7. (A) Mechanical properties testing of PEA and HPF where the ZnO film used for the preparation of HPF can be folded into a cranes shape. (B) Water contact angle testing of HPF surfaces. (C) Demonstration of HPF's self-cleaning effect.

In addition, the water contact angle of HPF is as high as 150.6° , hence the blue ink will not leave traces on the surface of HPF. It shows that HPF owns a certain self-cleaning ability (Figure 7B,C), which meets the requirements of construction or outdoor device shield applications.

5. Conclusions

A “heat pump film (HPF)” scheme was proposed and a two-layer material for cooling the covered object was developed. HPF, which is made of combined ZnO film and PE

bubble film by a simple scalable production process, has high solar reflection and infrared transmission characteristics. Additionally, the raw materials are easily available and low cost. Almost all common objects covered by HPF will be cooled by their own radiation to outside space with zero energy consumption. Theoretical and experimental proofs show that HPF has a favorable cooling effect: the object covered by HPF in outdoors cools down greater than 7 °C throughout the day, and there is still a cooling effect of greater than 3.5 °C under a high convection environment (56.9 W/m²/k).

HPF has certain strength (1.45 Mpa), good flexibility, bendability, and hydrophobic characteristics (the water contact angle, 150.6°). HPF is also easy to lay and install and is free from the limitations of the insulation box. HPF is suitable for widely applied scenarios, such as the building exterior surface, power base station cabinet, refrigerated transport vehicles cover.

The development of HPF can solve the practical application problem of radiation cooling technology to achieve ideal cooling in a high convection environment. Nevertheless, the performance of HPF continues to have much room for improvement. The infrared transmittance at 8–13 μm of the HPF cooler is being optimized and improved. According to deduction, a cooling effect of more than 20 °C can be achieved at a static environment, if some methods are adopted to increase the transmittance of HPF to 90%, such as applying spherical ZnO particles and fabricating with a complex fine mixing process. The wide application of HPF will make a contribution to global energy conservation and carbon reduction.

Supplementary Materials: The following supporting information can be downloaded at: <https://www.mdpi.com/article/10.3390/polym15010159/s1>, Supplementary Information S1: Heat Transfer Model for HPF; Figure S1: Conceptual model: Material's Infrared radiation distributes exponentially; Figure S2: Model calculation: The effect of the sun's absorption depth on the cooling performance of the radiator; Figure S3: Transmittance of PE, PP and POE film (all 25 μm thickness) over MIR wavelength; Figure S4: Evaluation of infrared transmission properties of different particles; Figure S5: Effect of particle size of ZnO on the normalized scattering cross section; Figure S6: Particle size testing of ZnO; Table S1: Various raw material price; Figure S7: Outdoor test experiment results of bubble films with different layers; Figure S8: Outdoor test experiment results of ZnO layer with different thickness; Figure S9: Measurement of transmittance of HPF and emissivity of PDMS; Table S2: Comparison between different testing devices; Figure S10: Standard Deviation (S) of all-day outdoor test results; Figure S11: Test of insulation effect of HPF; Figure S12: Outdoor windshield experiments; Figure S13: Outdoor cooling experiments on HPF-covered building materials; Figure S14: The cooling performance of the material at different emitted and absorbed solar powers; Figure S15: High convection environment tests; Figure S16: Model calculation: Effects of surface convection heat transfer coefficients and number of bubble film layers; Figure S17: Bending tests: HPF vs. PEA.

Author Contributions: Z.X., Z.M. and S.W. proposed the idea and conceptual design of the HPF and performed the theoretical work. Z.X., Z.M. and B.C. proposed the strategy for experimental design and analyzed the data. Z.M., Z.X. and B.C. completed the writing of the paper. Y.Z., W.G., B.C., Y.Z., B.L., C.C. and H.H. performed the experimental work. All authors have read and agreed to the published version of the manuscript.

Funding: This research was supported by the Zibo Key Research and Development Project (Grant 2021SNPT0004), the Fundamental Research Funds for the Central Universities (WUT: 2019III116CG), and the Key R & D projects of Hubei Province (No. 2021BAA174).

Institutional Review Board Statement: Not applicable.

Data Availability Statement: Not applicable.

Conflicts of Interest: The authors declare no conflict of interest.

References

1. IEA. *Flaring Emissions*; IEA: Paris, France, 2021; Available online: <https://www.iea.org/reports/flaring-emissions> (accessed on 8 May 2022).
2. Zinatloo-Ajabshir, S.; Salehi, Z.; Amiri, O.; Salavati-Niasari, M. Simple fabrication of Pr₂Ce₂O₇ nanostructures via a new and eco-friendly route; a potential electrochemical hydrogen storage material. *J. Alloy. Compd.* **2019**, *791*, 792–799. [CrossRef]

3. Zonarsaghar, A.; Mousavi-Kamazani, M.; Zinatloo-Ajabshir, S. Co-precipitation synthesis of CeVO₄ nanoparticles for electrochemical hydrogen storage. *J. Mater. Sci. Mater. Electron.* **2022**, *33*, 6549–6554. [CrossRef]
4. Dehghani, N.; Babamoradi, M.; Hajizadeh, Z.; Maleki, A. Improvement of Magnetic Property of CMC/Fe₃O₄ Nanocomposite by Applying External Magnetic Field During Synthesis. *Chem. Methodol.* **2020**, *4*, 92–99. [CrossRef]
5. Zinatloo-Ajabshir, S.; Morassaei, M.S.; Salavati-Niasari, M. Eco-friendly synthesis of Nd₂Sn₂O₇-based nanostructure materials using grape juice as green fuel as photocatalyst for the degradation of erythrosine. *Compos. Part B Eng.* **2019**, *167*, 643–653. [CrossRef]
6. Zinatloo-Ajabshir, S.; Morassaei, M.S.; Niasari, M.S. Facile fabrication of Dy₂Sn₂O₇-SnO₂ nanocomposites as an effective photocatalyst for degradation and removal of organic contaminants. *J. Colloid Interface Sci.* **2017**, *497*, 298–308. [CrossRef] [PubMed]
7. Zinatloo-Ajabshir, S.; Salavati-Niasari, M. Preparation of magnetically retrievable CoFe₂O₄@SiO₂@Dy₂Ce₂O₇ nanocomposites as novel photocatalyst for highly efficient degradation of organic contaminants. *Compos. Part B Eng.* **2019**, *174*, 106930. [CrossRef]
8. Zinatloo-Ajabshir, S.; Heidari-Asil, S.A.; Salavati-Niasari, M. Recyclable magnetic ZnCo₂O₄-based ceramic nanostructure materials fabricated by simple sonochemical route for effective sunlight-driven photocatalytic degradation of organic pollution. *Ceram. Int.* **2020**, *47*, 8959–8972. [CrossRef]
9. Etemadi, H.; Afsharkia, S.; Zinatloo-Ajabshir, S.; Shokri, E. Effect of alumina nanoparticles on the antifouling properties of polycarbonate-polyurethane blend ultrafiltration membrane for water treatment. *Polym. Eng. Sci.* **2021**, *61*, 2364–2375. [CrossRef]
10. Fan, G.; Ning, R.; Li, X.; Lin, X.; Du, B.; Luo, J.; Zhang, X. Mussel-Inspired Immobilization of Photocatalysts with Synergistic Photocatalytic-Photothermal Performance for Water Remediation. *ACS Appl. Mater. Interfaces* **2021**, *13*, 31066–31076. [CrossRef]
11. Cani, D.; van der Waal, J.C.; Pescarmona, P.P. Highly-accessible, doped TiO₂ nanoparticles embedded at the surface of SiO₂ as photocatalysts for the degradation of pollutants under visible and UV radiation. *Appl. Catal. A Gen.* **2021**, *621*, 118179. [CrossRef]
12. IEA. *Renewable Energy Policies in a Time of Transition: Heating and Cooling*; IEA: Paris, France, 2020; Available online: <https://www.iea.org/reports/renewable-energy-policies-in-a-time-of-transition-heating-and-cooling> (accessed on 8 May 2022).
13. IEA. *Cooling*; IEA: Paris, France, 2021; Available online: <https://www.iea.org/reports/cooling> (accessed on 8 May 2022).
14. Munday, J.N. Tackling Climate Change through Radiative Cooling. *Joule* **2019**, *3*, 2057–2060. [CrossRef]
15. Bongaarts, J. Intergovernmental Panel on Climate Change Special Report on Global Warming of 1.5 °C Switzerland: IPCC, 2018. *Popul. Dev. Rev.* **2019**, *45*, 251–252. [CrossRef]
16. Hossain, M.M.; Gu, M. Radiative Cooling: Principles, Progress, and Potentials. *Adv. Sci.* **2016**, *3*, 1500360. [CrossRef] [PubMed]
17. Bahadori, M.N. Passive Cooling Systems in Iranian Architecture. *Sci. Am.* **1978**, *238*, 144–155.
18. Berdahl, P. Radiative cooling with MgO and/or LiF layers. *Appl. Opt.* **1984**, *23*, 370–372. [CrossRef]
19. Granqvist, C.G.; Hjortsberg, A. Surfaces for radiative cooling: Silicon monoxide films on aluminum. *Appl. Phys. Lett.* **1980**, *36*, 139–141. [CrossRef]
20. Nilsson, T.M.; Niklasson, G.; Granqvist, C.G. A solar reflecting material for radiative cooling applications: ZnS pigmented polyethylene. *Sol. Energy Mater. Sol. Cells* **1992**, *28*, 175–193. [CrossRef]
21. Orel, B.; Gunde, M.K.; Krainer, A. Radiative cooling efficiency of white pigmented paints. *Sol. Energy* **1993**, *50*, 477–482. [CrossRef]
22. Bartoli, B.; Catalanotti, S.; Coluzzi, B.; Cuomo, V.; Silvestrini, V.; Troise, G. Nocturnal and diurnal performances of selective radiators. *Appl. Energy* **1977**, *3*, 267–286. [CrossRef]
23. Gentle, A.R.; Smith, G.B. Radiative Heat Pumping from the Earth Using Surface Phonon Resonant Nanoparticles. *Nano Lett.* **2010**, *10*, 373–379. [CrossRef]
24. Raman, A.P.; Anoma, M.A.; Zhu, L.; Rephaeli, E.; Fan, S. Passive radiative cooling below ambient air temperature under direct sunlight. *Nature* **2014**, *515*, 540–544. [CrossRef] [PubMed]
25. Li, X.; Peoples, J.; Huang, Z.; Zhao, Z.; Qiu, J.; Ruan, X. Full Daytime Sub-ambient Radiative Cooling in Commercial-like Paints with High Figure of Merit. *Cell Rep. Phys. Sci.* **2020**, *1*, 100221. [CrossRef]
26. Chen, Y.; Dang, B.; Fu, J.; Wang, C.; Li, C.; Sun, Q.; Li, H. Cellulose-Based Hybrid Structural Material for Radiative Cooling. *Nano Lett.* **2020**, *21*, 397–404. [CrossRef] [PubMed]
27. Zhang, H.; Ly, K.C.S.; Liu, X.; Chen, Z.; Yan, M.; Wu, Z.; Wang, X.; Zheng, Y.; Zhou, H.; Fan, T. Biologically inspired flexible photonic films for efficient passive radiative cooling. *Proc. Natl. Acad. Sci. USA* **2020**, *117*, 14657–14666. [CrossRef]
28. Cai, L.; Song, A.Y.; Li, W.; Hsu, P.; Lin, D.; Catrysse, P.B.; Liu, Y.; Peng, Y.; Chen, J.; Wang, H.; et al. Spectrally Selective Nanocomposite Textile for Outdoor Personal Cooling. *Adv. Mater.* **2018**, *30*, e1802152. [CrossRef]
29. Chen, G.; Wang, Y.; Qiu, J.; Cao, J.; Zou, Y.; Wang, S.; Ouyang, J.; Jia, D.; Zhou, Y. A visibly transparent radiative cooling film with self-cleaning function produced by solution processing. *J. Mater. Sci. Technol.* **2021**, *90*, 76–84. [CrossRef]
30. Masashi, O.; Chen, K.; Wei, L.; Fan, S. Self-adaptive radiative cooling based on phase change materials. *Opt. Express* **2018**, *26*, a777.
31. Fang, Z.; Ding, L.; Li, L.; Shuai, K.; Cao, B.; Zhong, Y.; Meng, Z.; Xia, Z. Thermal Homeostasis Enabled by Dynamically Regulating the Passive Radiative Cooling and Solar Heating Based on a Thermochromic Hydrogel. *ACS Photonics* **2021**, *8*, 2781–2790. [CrossRef]
32. Xia, Z.; Zhang, Z.; Meng, Z.; Yu, Z. A 24-hour thermoelectric generator simultaneous using solar heat energy and space cold energy. *J. Quant. Spectrosc. Radiat. Transf.* **2020**, *251*, 107038. [CrossRef]
33. Xia, Z.; Zhang, Z.; Meng, Z.; Ding, L.; Yu, Z. Thermoelectric Generator Using Space Cold Source. *ACS Appl. Mater. Interfaces* **2019**, *11*, 33941–33945. [CrossRef]

34. Trosseille, J.; Mongruel, A.; Royon, L.; Beysens, D. Radiative cooling for dew condensation. *Int. J. Heat Mass Transf.* **2021**, *172*, 121160. [[CrossRef](#)]
35. Chen, G.; Wang, Y.; Qiu, J.; Cao, J.; Zou, Y.; Wang, S.; Jia, D.; Zhou, Y. A facile bioinspired strategy for accelerating water collection enabled by passive radiative cooling and wettability engineering. *Mater. Des.* **2021**, *206*, 109829. [[CrossRef](#)]
36. Li, W.; Shi, Y.; Chen, K.; Zhu, L.; Fan, S. A Comprehensive Photonic Approach for Solar Cell Cooling. *ACS Photonics* **2017**, *4*, 774–782. [[CrossRef](#)]
37. Yoon, S.; Kim, M.; Seo, J.; Kim, S.; Lee, H.; Lee, J.; Lee, B.J. Performance analysis of a hybrid HVAC system consisting of a solar thermal collector and a radiative cooling panel. *Energy Build.* **2021**, *241*, 110921. [[CrossRef](#)]
38. Kang, M.H.; Lee, G.J.; Lee, J.H.; Kim, M.S.; Yan, Z.; Jeong, J.; Jang, K.; Song, Y.M. Outdoor-Useable, Wireless/Battery-Free Patch-Type Tissue Oximeter with Radiative Cooling. *Adv. Sci.* **2021**, *8*, 2004885. [[CrossRef](#)]
39. Goldstein, E.A.; Raman, A.P.; Fan, S. Sub-ambient non-evaporative fluid cooling withthesky. *Nat. Energy* **2017**, *2*, 143. [[CrossRef](#)]
40. Tian, Y.; Shao, H.; Liu, X.; Chen, F.; Li, Y.; Tang, C.; Zheng, Y. Superhydrophobic and Recyclable Cellulose-Fiber-Based Composites for High-Efficiency Passive Radiative Cooling. *ACS Appl. Mater. Interfaces* **2021**, *13*, 22521–22530. [[CrossRef](#)]
41. Kang, H.; Qiao, Y.; Li, Y.; Qin, W.; Wu, X. Keep Cool: Polyhedral ZnO@ZIF₈ Polymer Coatings for Daytime Radiative Cooling. *Ind. Eng. Chem. Res.* **2020**, *59*, 15226–15232. [[CrossRef](#)]
42. Li, X.; Peoples, J.; Yao, P.; Ruan, X. Ultrawhite BaSO₄ Paints and Films for Remarkable Daytime Subambient Radiative Cooling. *ACS Appl. Mater. Interfaces* **2021**, *13*, 21733–21739. [[CrossRef](#)]
43. Zu, M.; Yan, F.; Lv, C.; Li, M.; Hu, W.; Cheng, H. Daytime passive radiative cooler using zeolite. *J. Porous Mater.* **2021**, *29*, 1–8. [[CrossRef](#)]
44. Zhai, Y.; Ma, Y.; David, S.N.; Zhao, D.; Lou, R.; Tan, G.; Yang, R.; Yin, X. Scalable-manufactured randomized glass-polymer hybrid metamaterial for daytime radiative cooling. *Science* **2017**, *355*, 1062–1066. [[CrossRef](#)] [[PubMed](#)]
45. Yoon, T.Y.; Son, S.; Min, S.; Chae, D.; Woo, H.Y.; Chae, J.-Y.; Lim, H.; Shin, J.; Paik, T.; Lee, H. Colloidal deposition of colored daytime radiative cooling films using nanoparticle-based inks. *Mater. Today Phys.* **2021**, *21*, 100510. [[CrossRef](#)]
46. Banik, U.; Agrawal, A.; Meddeb, H.; Sergeev, O.; Reininghaus, N.; Götz-Köhler, M.; Gehrke, K.; Stührenberg, J.; Vehse, M.; Sznajder, M.; et al. Efficient Thin Polymer Coating as a Selective Thermal Emitter for Passive Daytime Radiative Cooling. *ACS Appl. Mater. Interfaces* **2021**, *13*, 24130–24137. [[CrossRef](#)]
47. Liu, Y.; Bai, A.; Fang, Z.; Ni, Y.; Lu, C.; Xu, Z. A Pragmatic Bilayer Selective Emitter for Efficient Radiative Cooling under Direct Sunlight. *Materials* **2019**, *12*, 1208. [[CrossRef](#)] [[PubMed](#)]
48. Smith, G. Amplified radiative cooling via optimised combinations of aperture geometry and spectral emittance profiles of surfaces and the atmosphere. *Sol. Energy Mater. Sol. Cells* **2009**, *93*, 1696–1701. [[CrossRef](#)]
49. Chen, Z.; Zhu, L.; Raman, A.; Fan, S. Radiative cooling to deep sub-freezing temperatures through a 24-h day–night cycle. *Nat. Commun.* **2016**, *7*, 13729. [[CrossRef](#)]
50. Chen, G.; Wang, Y.; Qiu, J.; Cao, J.; Zou, Y.; Wang, S.; Jia, D.; Zhou, Y. Robust Inorganic Daytime Radiative Cooling Coating Based on a Phosphate Geopolymer. *ACS Appl. Mater. Interfaces* **2020**, *12*, 54963–54971. [[CrossRef](#)]
51. Wang, T.; Wu, Y.; Shi, L.; Hu, X.; Chen, M.; Wu, L. A structural polymer for highly efficient all-day passive radiative cooling. *Nat. Commun.* **2021**, *12*, 365–20646. [[CrossRef](#)]
52. Yang, Z.; Zhang, J. Bioinspired Radiative Cooling Structure with Randomly Stacked Fibers for Efficient All-Day Passive Cooling. *ACS Appl. Mater. Interfaces* **2021**, *13*, 43387–43395. [[CrossRef](#)]
53. Cheng, Z.; Han, H.; Wang, F.; Yan, Y.; Shi, X.; Liang, H.; Zhang, X.; Shuai, Y. Efficient radiative cooling coating with biomimetic human skin wrinkle structure. *Nano Energy* **2021**, *89*, 106377. [[CrossRef](#)]
54. Kim, H.; McSherry, S.; Brown, B.; Lenert, A. Selectively Enhancing Solar Scattering for Direct Radiative Cooling through Control of Polymer Nanofiber Morphology. *ACS Appl. Mater. Interfaces* **2020**, *12*, 43553–43559. [[CrossRef](#)]
55. Chen, X.; He, M.; Feng, S.; Xu, Z.; Peng, H.; Shi, S.; Liu, C.; Zhou, Y. Cellulose-based porous polymer film with auto-deposited TiO₂ as spectrally selective materials for passive daytime radiative cooling. *Opt. Mater.* **2021**, *120*, 111431. [[CrossRef](#)]
56. Tang, K.; Dong, K.; Li, J.; Gordon, M.P.; Reichertz, F.G.; Kim, H.; Rho, Y.; Wang, Q.; Lin, C.-Y.; Grigoropoulos, C.P.; et al. Temperature-adaptive radiative coating for all-season household thermal regulation. *Science* **2021**, *374*, 1504–1509. [[CrossRef](#)]
57. Wang, S.; Wang, Y.; Zou, Y.; Chen, G.; Ouyang, J.; Jia, D.; Zhou, Y. Biologically Inspired Scalable-Manufactured Dual-layer Coating with a Hierarchical Micropattern for Highly Efficient Passive Radiative Cooling and Robust Superhydrophobicity. *ACS Appl. Mater. Interfaces* **2021**, *13*, 21888–21897. [[CrossRef](#)]
58. Lin, K.; Chao, L.; Ho, T.C.; Lin, C.; Chen, S.; Du, Y.; Huang, B.; Tso, C.Y. A flexible and scalable solution for daytime passive radiative cooling using polymer sheets. *Energy Build.* **2021**, *252*, 111400. [[CrossRef](#)]
59. Li, X.; Sun, B.; Sui, C.; Nandi, A.; Fang, H.; Peng, Y.; Tan, G.; Hsu, P.C. Integration of daytime radiative cooling and solar heating for year-round energy saving in buildings. *Nat. Commun.* **2020**, *11*, 6101. [[CrossRef](#)] [[PubMed](#)]
60. Gamage, S.; Banerjee, D.; Alam, M.; Hallberg, T.; Åkerlind, C.; Sultana, A.; Shanker, R.; Berggren, M.; Crispin, X.; Kariis, H.; et al. Reflective and transparent cellulose-based passive radiative coolers. *Cellulose* **2021**, *28*, 9383–9393. [[CrossRef](#)]
61. Zeng, S.; Pian, S.; Su, M.; Wang, Z.; Wu, M.; Liu, X.; Chen, M.; Xiang, Y.; Wu, J.; Zhang, M.; et al. Hierarchical-morphology metafabric for scalable passive daytime radiative cooling. *Science* **2021**, *373*, 692–696. [[CrossRef](#)]

62. Leroy, A.; Bhatia, B.; Kelsall, C.C.; Castillejo-Cuberos, A.; Di Capua H, M.; Zhao, L.; Zhang, L.; Guzman, A.M.; Wang, E.N. High-performance subambient radiative cooling enabled by optically selective and thermally insulating polyethylene aerogel. *Sci. Adv.* **2019**, *5*, eaat9480. [[CrossRef](#)]
63. Bond, W.L. Measurement of the Refractive Indices of Several Crystals. *J. Appl. Phys.* **1965**, *36*, 1674–1677. [[CrossRef](#)]
64. Querry, M.R. *Optical Constants 1985, Contractor Report CRDC-CR-85034*; Missouri University: Kansas City, MO, USA, 1985.
65. Zhou, L.; Song, H.; Liang, J.; Singer, M.; Zhou, M.; Stegenburgs, E.; Zhang, N.; Xu, C.; Ng, T.; Yu, Z.; et al. A polydimethylsiloxane-coated metal structure for all-day radiative cooling. *Nat. Sustain.* **2019**, *2*, 718–724. [[CrossRef](#)]
66. Han, D.; Fei, J.; Li, H.; Ng, B.F. The criteria to achieving sub-ambient radiative cooling and its limits in tropical daytime. *Build. Environ.* **2022**, *221*, 109281. [[CrossRef](#)]

Disclaimer/Publisher's Note: The statements, opinions and data contained in all publications are solely those of the individual author(s) and contributor(s) and not of MDPI and/or the editor(s). MDPI and/or the editor(s) disclaim responsibility for any injury to people or property resulting from any ideas, methods, instructions or products referred to in the content.